Institut für Numerische Simulation
Rheinische Friedrich-Wilhelms-Universität Bonn

Wegelerstraße 6 • 53115 Bonn • Germany
phone +49 228 73-3427 • fax +49 228 73-7527
www.ins.uni-bonn.de

M. Griebel, A. Rüttgers

Simulation of dilute polymeric fluids in a three-dimensional contraction using a multiscale FENE model

INS Preprint No. 1308

April 2013

SIMULATION OF DILUTE POLYMERIC FLUIDS IN A THREE-DIMENSIONAL CONTRACTION USING A MULTISCALE FENE MODEL

M. Griebel[1] and A. Rüttgers[1]

[1]*Institute for Numerical Simulation, University of Bonn, Germany – {griebel, ruettgers}@ins.uni-bonn.de*

Abstract – We apply the multiscale FENE model to a 3D square-square contraction flow problem. For this purpose, we couple the stochastic Brownian configuration field method (BCF) with our fully parallelized three-dimensional Navier-Stokes solver NaSt3DGPF. The robustness of the BCF method enables the numerical simulation of high Deborah number flows for which most macroscopic methods suffer from stability issues. We compare the results of our simulations with that of experimental measurements from literature and obtain a very good agreement. In particular, we are able to reproduce effects such as strong vortex enhancement, streamline divergence and flow inversion for highly elastic flows. Due to their computational complexity, our simulations require massively parallel computations. Using a domain decomposition approach with MPI, we achieve excellent scale-up results for up to 128 processors.

Keywords: dilute polymeric fluids, multiscale method, Brownian configuration fields, FENE model, parallel computing

Introduction

The computational modeling of dilute polymeric fluids usually involves an additional polymeric stress tensor in the Navier-Stokes equations and an additional system of differential equations for the stress tensor entries, compare the Oldroyd-B or the Phan-Thien Tanner (PTT) model. After discretization, these macroscopic models are often restricted in their scope of application due to numerical instabilities that appear beyond a critical Deborah or Weissenberg number (cf. high Weissenberg number problem).

One attempt to overcome this problem is multiscale modeling. This approach directly solves the kinetic equations of the microscopic system. Most multiscale methods used in practice are variants of the particle-based CONNFFESSIT technique by Laso and Öttinger [1] or of the grid-based Brownian Configuration field (BCF) method by Hulsen et al. [2]. Both approaches employ stochastics for the representation of polymeric configurations. Using Monte-Carlo integration, the macroscopic stress tensor is obtained as the first moment of the polymer configurations. Keunings gives a detailed overview of various micro-macro approaches in [3]. In the following, we present, to the best of our knowledge, the first 3D multiscale FENE (**f**initely **e**xtensible **n**onlinear **e**lastic) simulations for square-square contraction flows and compare our results with that from laboratory experiments. Our multiscale simulations are more stable than comparable macroscopic simulations for high Deborah numbers.

The remainder of this article is organized as follows: We first state the multiscale model equations and describe their discretization. Next, we illustrate the 3D contraction geometry and compare our simulation results with experimental results from literature. At last, we evaluate our findings and discuss possible extensions.

Governing equations for the multiscale model

The macroscopic 3D Navier-Stokes equations for an incompressible fluid are

$$\frac{\partial \boldsymbol{u}}{\partial t} + \boldsymbol{u} \cdot \nabla \boldsymbol{u} = -\nabla p + \frac{1}{Re}\beta \Delta \boldsymbol{u} + \frac{1}{Re}\nabla \cdot \boldsymbol{\tau_p} \qquad (1)$$

$$\nabla \cdot \boldsymbol{u} = 0\,, \qquad (2)$$

where Re denotes the dimensionless Reynolds number, β the ratio of polymer to total viscosity, and τ_p the additional polymeric stress tensor. Additionally, Eq. 1 and Eq. 2 have to be complemented with initial and boundary conditions for the velocity field $\boldsymbol{u}$ and the pressure p.

On the micro-scale we employ dumbbell systems immersed in a Newtonian solvent for approximating a dilute polymeric fluid. The dumbbell consists of two separate masses connected with a nonlinear FENE spring. The dumbbell model is illustrated in Fig. 1.

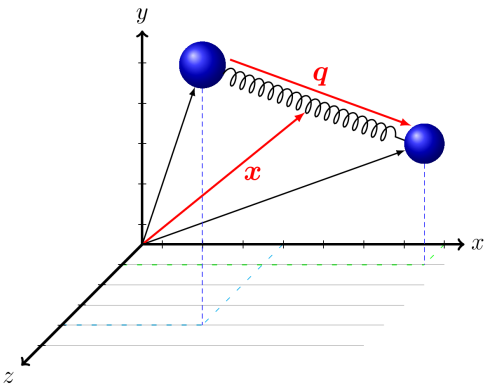

Figure 1 – A position vector $\boldsymbol{x} \in \mathbb{R}^3$ and the orientation $\boldsymbol{q} \in \mathbb{R}^3$ are sufficient for a complete description of the dumbbell in the 3D flow domain.

The BCF method applies a stochastic process $\boldsymbol{Q_t}$ to evolve the dumbbell's orientation $\boldsymbol{q}$ in time. The corresponding stochastic differential equation is

$$d\boldsymbol{Q_t} = \left(-\boldsymbol{u}\nabla_x\boldsymbol{Q_t} + (\nabla_x\boldsymbol{u})^T\boldsymbol{Q_t} - \frac{1}{2\,De}\boldsymbol{F}(\boldsymbol{Q_t})\right)dt + \sqrt{\frac{1}{De}}d\boldsymbol{W_t}\,, \tag{3}$$

where $d\boldsymbol{W_t}$ denotes a three-dimensional stochastic process to model Brownian forces. Eq. 3 involves a dimensionless Deborah number *De* to describe the elasticity of the fluid. The term $\boldsymbol{F}(\boldsymbol{Q_t})$ denotes the FENE spring force which is defined as

$$\boldsymbol{F}(\boldsymbol{Q_t}) = \frac{\boldsymbol{Q_t}}{1 - \| \boldsymbol{Q_t} \|^2/b}, \tag{4}$$

where *b* is a parameter for the maximum dumbbell extension. Finally, Kramers' relation

$$\boldsymbol{\tau_p} = \frac{C(1-\beta)}{De}(\langle \boldsymbol{Q_t} \otimes \boldsymbol{F}(\boldsymbol{Q_t})\rangle - \boldsymbol{Id}) \tag{5}$$

couples the stochastic processes on the micro-scale with the polymeric stress tensor $\boldsymbol{\tau_p}$ in Eq. 1. We use $\boldsymbol{Id}$ in Eq. 5 to denote the identity matrix and *C* to describe a dimension-dependent constant, which relates to the spring force potential.

Numerical discretization

We discretize the Navier-Stokes equations Eq. 1-2 in space with a second-order finite difference scheme. For this purpose, we subdivide the flow domain into rectangular grid cells and evaluate the unknowns $\boldsymbol{u}$, p and $\boldsymbol{\tau_p}$ on a staggered grid. Furthermore, we decouple pressure and velocity field by using Chorin's projection method which is described in [4]. Since the following problems invoke low Reynolds numbers, we employ an implicit 2nd-order Crank-Nicolson scheme for the diffusive terms in Eq. 1 to avoid time step restrictions. A more detailed description is given in Griebel et al. [5] and Croce et al. [6].

We solve Eq. 3 for a number of $i = 1, \dots, N$ sample particles $\boldsymbol{Q_t^{(i)}}$ per grid cell, the Brownian configuration fields, which are distributed according to a specific density function for the FENE model. Using Monte Carlo integration we approximate the expectation in Eq. 5 with these configuration fields. Due to the stochastic treatment, the stress tensor solution exhibits stochastic noise. Furthermore, we perform the temporal discretization with an Euler-Maruyama scheme that is implicit in the spring force term. For a detailed description of its implementation in NaSt3DGPF and a multiscale code validation with an analytical benchmark solution we refer to Rüttgers [7].

Three-dimensional contraction simulations

We consider square-square contraction flows in which the fluid enters the domain in a quadratic channel with side length $2H_1 = 24\ mm$ and contracts into a smaller channel with side length $2H_2 = 6mm$ (contraction ratio 4:1). These parameters are chosen according to the experimental measurements by Sousa et al. [8] to allow for comparisons. One important aspect of the square-square contraction flow geometry is the occurrence of 3D flow patterns in contrast to 2D axisymmetric or planar contraction flows.

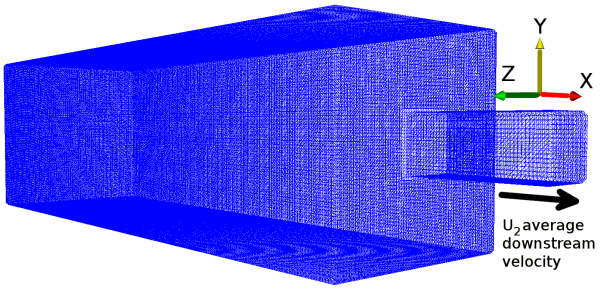

Figure 2 – Illustration of the 3D simulation domain.

In Fig. 2 we illustrate the simulation domain. The upstream channel length is $82.5mm$; the length of the downstream channel is $15mm$. This results in an overall simulation domain of $97.5mm \times 24mm \times 24mm$. The complete grid consists of $260 \times 64 \times 64$ grid cells which results in a mesh width of $h = 0.375mm$. To our knowledge, this resolution is higher than for any comparable multiscale simulation up to now.

The most CPU-intensive aspects of the simulation are the stochastic terms on the micro-scale. Each grid cell contains $N = 800$ stochastic variables which leads to a total number of $800 \times 260 \times 64 \times 64 \approx 850 \cdot 10^6$ configuration fields. If we use double precision machine numbers for each of the three BCF components, the total memory requirement is approximately 19 GB.

We adapt the specifications of Sousa et al. [8] for a shear-thinning viscoelastic fluid that consists of 40% glycerol, 59.9% water and PAA at a weight concentration of $600\ ppm$. The authors characterize the fluid as follows: fluid density $\rho = 1156\ kg\ m^{-3}$, solvent shear viscosity $\eta_s = 0.03\ Pa \cdot s$, zero polymer shear viscosity $\eta_p = 1.62\ Pa \cdot s$ and fluid relaxation time $\lambda = 32s$. Using these values, we derive $\beta = 0.0182$ for Eq. 1 and Eq. 5. Next, we prescribe the Reynolds and Deborah numbers in Eq. 1, Eq. 3 and Eq. 5 in terms of the average downstream velocity U_2 and half of the downstream channel width $H_2 = 3mm$. To this end, we define

$$Re_2 = \frac{\rho U_2 (2H_2)}{\eta_s + \eta_p} \quad \text{and} \quad De_2 = \frac{\lambda U_2}{H_2} \tag{6}$$

and choose for three multiscale simulations the average velocities $U_2 = 2.26mm\ s^{-1}$, $10.1mm\ s^{-1}$ and $14.7mm\ s^{-1}$, respectively. Thus, we obtain the Deborah numbers 24.1, 108 and 157 as in Sousa

et al. [8]. Note that we have added the lower index 2 to indicate that De_2 is defined using the downstream channel's characteristics. In all cases the Reynolds number is below 1 and, therefore, elasticity instead of inertia is the dominant effect in the simulations.

The FENE dumbbell extension parameter b is an additional degree of freedom in the system of Eq. 1-5. This parameter allows a characterization of the fluid's shear-thinning behavior. The characteristic shear rate $\dot{\gamma} = U_2/H_2$ of the simulations ranges from $0.75\ s^{-1}$ to $4.9\ s^{-1}$. In this interval we compare different values of b and look for the best fit to the simplified Phan-Thien Tanner (SPTT) model in Sousa et al. [8]. The results in Fig. 3 for the SPTT model (dark blue) are in agreement with FENE $b = 20$ (green) for the stress coefficient ψ_1. Therefore, we fix $b = 20$ for our simulations from now on.

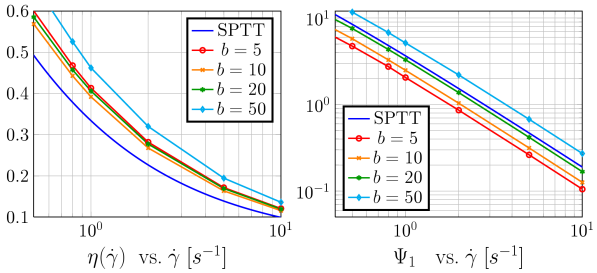

Figure 3 – Visualization of the shear viscosity $\eta = \eta_p + \eta_s$ over $\dot{\gamma}$ (left) and of the first stress coefficient $\psi_1$over $\dot{\gamma}$ (right).

Parallelization

All numerical simulations have been computed on the high performance cluster (HPC) *Siebengebirge* of the Institute for Numerical Simulation at the University of Bonn. This HPC cluster features 5 computing nodes with 160 CPUs and a main memory of 2560 GB in total. The Linpack performance of the system is 1349 GFlops/s with a parallel efficiency of 93%. Each computation required 10-14 weeks on 64 CPUs which illustrates the huge computational requirements of fully 3D multiscale simulations. In Tab. 1 we list the scale-up behavior of our implementation for a test problem. Since the BCF model can be parallelized efficiently, the achieved results are nearly optimal.

Table 1 – Scale-up behavior using NaSt3DGPF with BCFs for 1 up to 128 processors. Each processor computes a subdomain of $10 \times 20 \times 20$ grid cells.

CPU number	computation time [s]	scale-up
1	232	1.0
2	227	1.0
4	238	0.98
8	247	0.94
16	253	0.92
32	255	0.91
64	272	0.85
128	301	0.77

Numerical results

An increase of the fluid's elasticity leads to a strong vortex enhancement. We now present the flow field on the central plane $z = 0.012m$ for two different Deborah numbers. In Fig. 4 the case of $De_2 = 24.1$ is given. We indicate the boundary of the upper vortex by a white dashed line and furthermore give a typical streamline by the solid grey line. Results for $De_2 = 157$ are shown in Fig. 5. Here, we observe streamline divergence which coincides with the findings of Sousa et al. [8].

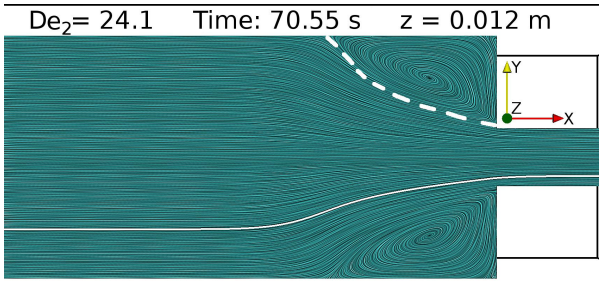

Figure 4 – Simulation result for $De_2 = 24.1$ at time $t = 70.55\ s$ visualized on the central plane $z = 0.012m$.

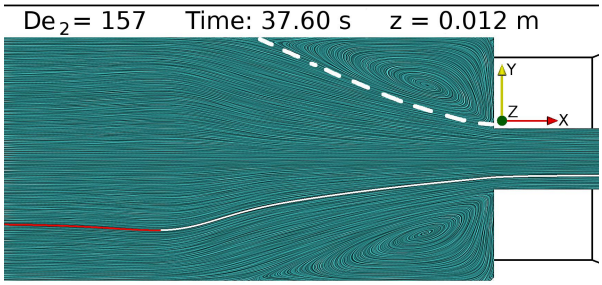

Figure 5 – Simulation result for $De_2 = 157$ at time $t = 37.60\ s$ on the central plane $z = 0.012m$. The divergence of the streamline is indicated in red.

It is important to recognize the system's steady state to avoid additional costs and thus to cut down the computational complexity of the simulations. For this reason, we visualize the normalized vortex lengths $x_R/2H_1$ in Fig. 6 on the central plane $z = 0.012m$ over time. For all three Deborah numbers the plot shows a plateau, i.e. all simulations have reached a steady state. We give a qualitative comparison for the results in Tab. 2. For $De_2 = 24.1$ there is a high level of agreement between the findings by Sousa et al. [8] and our simulations. We performed further macroscopic simulations (PTT) with Deborah numbers in the order of $\mathcal{O}(1)$ which confirmed this good agreement of the measured vortex lengths for flows with low elasticity. On the other hand, for the higher Deborah numbers of 108 and 157, respectively, the numerical scheme clearly underestimates the measured experimental vortex sizes. Note, however, that classical macroscopic approaches severely suffer from numerical instabilities

when simulating Deborah numbers of order $\mathcal{O}(100)$ and do not obtain comparable values at all. Furthermore, it is not quite clear to us how large the measured laboratory error is for the case of the higher Deborah numbers.

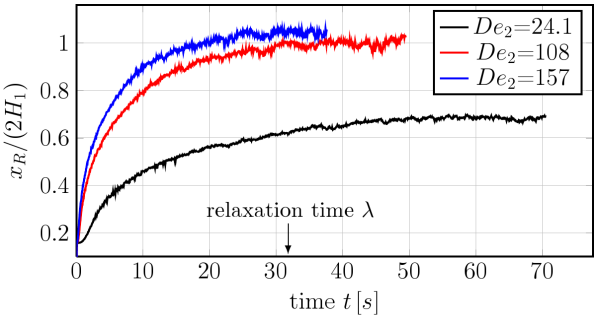

Figure 6 – Plot of the normalized vortex lengths $x_R/2H_1$ over time for different Deborah numbers. The vortices have reached a steady state.

Table 2 – Comparison of experimental vortex lengths from Sousa et al. [8] with our FENE simulation results.

Deborah De_2	24.1	108	157
Sousa et al. [8]	≈ 0.8	≈ 1.8	≈ 2.4
FENE	≈ 0.7	≈ 1.0	≈ 1.05

In Fig. 7 we compare the axial velocity profiles on the channel centerline $(x, 0.012m, 0.012m)$. Again, there is a good agreement for $De_2 = 24.1$ but a discrepancy for higher Deborah numbers. Since the vortices for $De_2 = 108$ in the laboratory experiment are larger in size, the fluid starts to accelerate earlier. Moreover, for $De_2 = 108$ we observe a slight velocity undershoot before the fluid starts to accelerate (cf. inset in Fig. 7) which is also reported in Sousa et al. [8].

Literature findings often state a vortex structure for highly elastic flows which is inversely oriented to that of nearly Newtonian flows. Fig. 8 compares the streamlines in the case of $De_2 = 1.0$ (macroscopic PTT with NaSt3DGPF) and $De_2 = 157$. The red cross indicates the starting area of the streamlines in both flows. For $De_2 = 1.0$ the streamlines rotate, beginning at the channel corners, by 45°. In contrast, the streamlines for $De_2 = 157$ rotate the other way round but end in these corners before going through the contraction. Clearly, these flow phenomena are 3D effects.

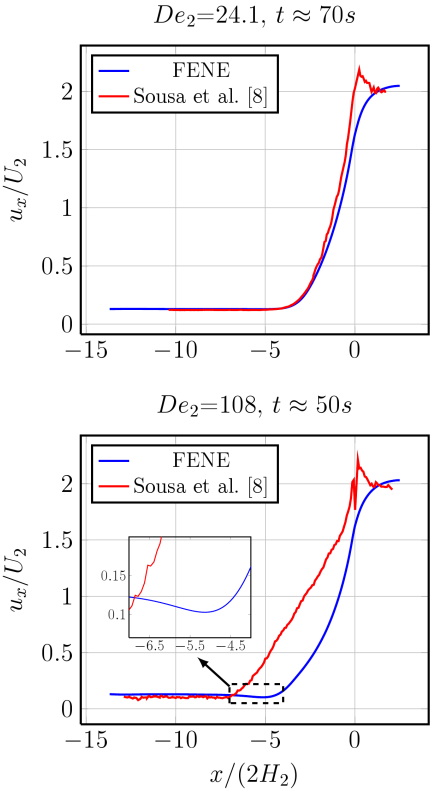

Figure 7 – Axial velocity profiles at the channel centerline. We use $U_2 = 2.26mm/s$ $(De_2 = 24.1)$ and $U_2 = 10.1mm/s$ $(De_2 = 108)$ for proper scaling.

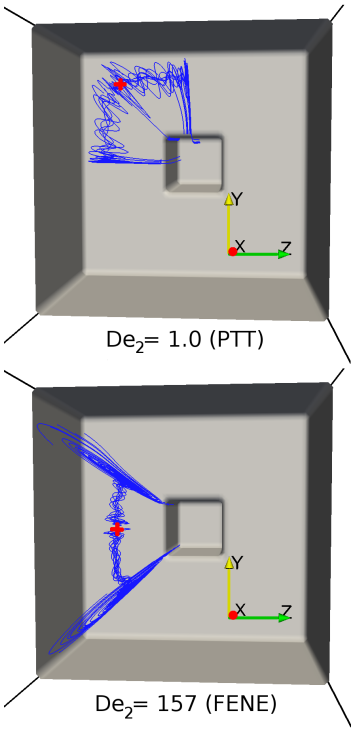

Figure 8 – In contrast to flows with low elasticity (top) the flow direction is inversed for high Deborah number flows (bottom). Note that the perspective coincides with the flow direction and that the upstream channel is clipped.

At last, we present results for the first normal stress component τ_{xx}. As reported by Keunings [3] for the BCF method, the stress field is smooth in space at a fixed point in time (cf. Fig. 9). On the other hand, plotting the stress tensor over time clearly shows the stochastic behavior of the solution which is reduced for a larger number of samples *N* (cf. Fig. 10). We obtain comparable results for the other stress components.

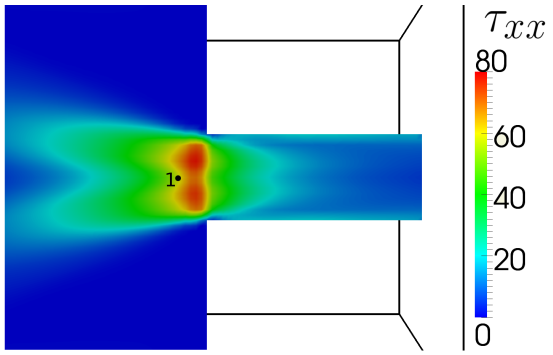

Figure 9 – First normal stress component τ_{xx} on the slice $z = 0.012m$ at $t \approx 50s$ for $De_2 = 108$.

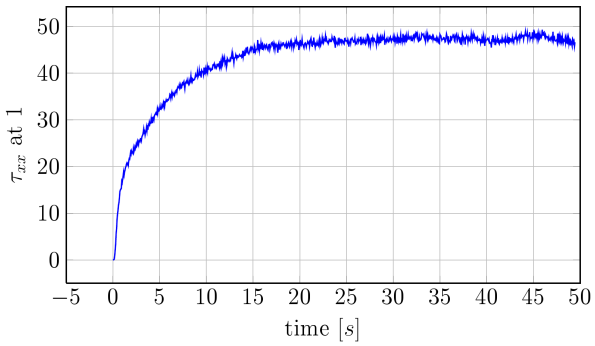

Figure 10 – First normal stress component τ_{xx} plotted over time at position 1 of Fig. 9. Due to the stochastic treatment, the τ_{xx}-component exhibits stochastic noise.

Conclusions

3D square-square contraction flows were numerically studied for a multiscale FENE dumbbell model using the Brownian configuration field approach. The simulations clearly show an increased numerical stability compared to classical macroscopic methods. This coincides with other findings for the BCF method. While there is a good agreement for lower Deborah numbers, the model fails to accurately predict the actual vortex sizes for higher Deborah numbers. One reason might lie in the single-mode FENE model itself. The description of real fluids often requires multi-mode FENE models which, due to their huge computational complexity, have not been tackled with multiscale methods yet. Nevertheless, our results indicate the potential of multiscale model approaches for the simulation of polymeric fluids. This will however invoke massively parallel computing.

Acknowledgements

The authors wish to thank Dr. P.C. Sousa from University of Porto, Portugal, for the fruitful discussions and for providing the experimental velocity profiles used in Fig. 7.

References

1. M. Laso; H.C. Öttinger *J. Non-Newt. Fluid Mech.* 1993**,** *47,* 1-20.
2. M.A. Hulsen; A.G.P. van Heel; B.H.A.A. van den Brule *J. Non-Newt. Fluid Mech.* 1997**,** *70,* 79-101.
3. R. Keunings in *Rheology Reviews,* D.M. Binding and K.Walters, Ed.; British Society of Rheolgy, 2004; 67-98.
4. A.J. Chorin *Math. Comp.* 1968**,** *22,* 745-762.
5. M. Griebel; T. Dornseifer; T. Neunhoeffer, *Numerical Simulation in Fluid Dynamics, a Practical Introduction,* SIAM, Philadelphia, 1998.
6. R. Croce; M. Griebel; M.A. Schweitzer *Int. J. Numer. Meth. Fluids* 2009**,** *62(9),* 963-993.
7. A. Rüttgers, Diploma Thesis, University of Bonn, 2010.
8. P.C. Sousa; P.M. Coelho, M.S.N. Oliveira, M.A. Alves *Chem. Eng. Sci.* 2011**,** *66,* 998-100.